

Article

Designs of Miniature Optomechanical Sensors for Measurements of Acceleration with Frequencies of Hundreds of Hertz

Marina Reznikina^{1,2,*}  and Claus Braxmaier^{1,3} 

¹ Institute for Microelectronics, University of Ulm, 2022 Albert–Einstein–Allee 43, 89081 Ulm, Germany; claus.braxmaier@uni-ulm.de

² Theoretical Electrical Technique Department, National Technical University “Kharkiv Polytechnic Institute”, 2 Kyrpychova Str., 61002 Kharkiv, Ukraine

³ Department of Quantum Metrology, Institute for Quantum Technologies, German Aerospace Center (DLR e.V.), 2022 Wilhem–Runge–Straße 10, 89081 Ulm, Germany

* Correspondence: maryna.rezynkina@uni-ulm.de

Abstract: Some applications, such as aerospace testing and monitoring the operating conditions of equipment on space missions, require mechanical sensors capable of measuring accelerations at frequencies of several hundred hertz. For such measurements, optomechanical sensors can be used, providing the ability to measure accelerations without calibration. To enable such measurements, improved designs of drum-type sensors with the assigned performance have been elaborated. Such designs make it possible to provide the necessary levels of natural frequencies for optomechanical sensors and eliminate crosstalk. Using mathematical modeling, the dependencies of the mechanical characteristics of the proposed types of acceleration sensors versus their parameters were obtained. The use of such sensor designs ensures their compactness, making their manufacturing more technologically sound and suitable for use, in particular, in space missions.

Keywords: acceleration sensors design; mechanical characteristics; optomechanical accelerometers; crosstalk; numerical modeling



Citation: Reznikina, M.; Braxmaier, C. Designs of Miniature Optomechanical Sensors for Measurements of Acceleration with Frequencies of Hundreds of Hertz. *Designs* **2024**, *8*, 67. <https://doi.org/10.3390/designs8040067>

Academic Editors: Mahdi Bodaghi and Richard Drevet

Received: 29 May 2024

Revised: 27 June 2024

Accepted: 1 July 2024

Published: 4 July 2024



Copyright: © 2024 by the authors. Licensee MDPI, Basel, Switzerland. This article is an open access article distributed under the terms and conditions of the Creative Commons Attribution (CC BY) license (<https://creativecommons.org/licenses/by/4.0/>).

1. Introduction

Optomechanical inertial sensors (OMIS) are being widely investigated as they allow for accurate measurements over long periods and do not require calibration [1]. They are resistant to electromagnetic interference [2] and allow acceleration measurements to be made in a wide frequency range from fractions of hertz to tens of kilohertz [3,4]. This technology is used in space missions for navigation applications [1], for geodesy [5], for testing and metrology [3], etc.

An optical Fabry–Perot resonator is used to measure acceleration using optical–mechanical sensors. One of the resonator mirrors is located on the movable test mass of the OMIS, and the second mirror is connected to the fixed part of the sensor and is motionless relative to the test mass [5]. Both mirrors must be polished. When acceleration is applied to such a system, the test mass moves, and the length of the Fabry–Perot cavity changes. This change in length is measured by an optical cavity reading [1].

The advantages of OMIS over other acceleration measurement technologies are determined by their compact size and light weight, as well as the ability to optically read measurement results [6]. These advantages of OMIS are especially relevant in space missions, where the sensors must ensure high measurement accuracy, be miniature, resistant to electromagnetic interference, allow for the measurement of accelerations that quickly change over time, and provide long-term operation without calibration [7].

The used designs of the optomechanical accelerometer are monolithic fused silica oscillators consisting of a parallelepiped proof mass that is fastened by two flexible thin consoles to the outer constrained frame—the so-called in-plane OMIS [1,5,8]. Another

type of design is drum-type construction with a cylindrical proof mass in the middle connected to the outer constrained hollow cylinder by four [1,5,9] or three [10,11] thin consoles—flexures—the so-called out-of-plane OMIS. These designs are used for measuring accelerations at higher frequencies.

Some applications, such as vibration testing, launcher acceleration spectrum measurements, and acceleration measurements in space, require acceleration measurements at frequencies up to several hundred hertz. Since the operating frequency must be approximately an order of magnitude smaller than the first natural frequency of the OMIS, to measure accelerations at such frequencies, the first natural frequency must be on the order of several kilohertz.

Manufacturing monolithic OMIS from a single block of fused silica is necessary to provide its stiffness and durability, but it is a technologically complex and expensive process. Therefore, as a rule, the production of not one OMIS sample but a series of them is ordered. In this case, it is advisable to first carry out mathematical modeling of mechanical processes in OMIS of various designs with various parameters to select optimal constructions. As criteria for OMIS compliance with the requirements, one should consider such characteristics as its natural frequencies and crosstalk levels, as well as technological possibilities for manufacturing, subsequent polishing, and control of the geometric dimensions of a sample of the selected design.

For a number of applications, in particular when testing space technology objects, as well as when measuring acceleration in space (measured acceleration frequencies up to several hundred hertz), when reading displacements, it is necessary to use Fabry–Perot cavities with large finesse values. In this case, the mirrors of the Fabry–Perot cavity must be well polished. Since one of the mirrors of such a cavity is the front surface of the test mass, it is necessary to ensure its high-quality polishing. Existing OMIS designs are typically used with Fabry–Pérot cavities, which have low finesse values and therefore do not require special coatings and subsequent polishing to be applied to their front surface. In addition to selecting parameters that provide the required mechanical characteristics of the OMIS, when developing the design, it is necessary to take into account the possibility of its manufacture using existing technological means. As experimental studies have shown, high-quality polishing of the front surface of the OMIS test mass is technologically possible when the size of the gap between test mass 1 and the outer constrained cylinder is reduced. Another possibility to ensure such high-quality polishing is to make the entire front surface of OMIS, which includes its moving and stationary parts, almost continuous so that during polishing, the front surface remains practically motionless. As will be shown below, existing drum-type OMIS designs in the frequency range under consideration do not provide such high-quality polishing capabilities. In this regard, there is a need to develop new OMIS designs, since without this, the implementation of OMIS operating in the frequency range up to hundreds of hertz and using Fabry–Pérot cavities with large finesse values for optical reading is impossible.

The purpose of this work is to select, using numerical modeling of mechanical processes in OMIS, their design and geometric parameters that provide an operating frequency range of several hundred hertz. It is expected that such OMIS will provide the ability to polish the surface of their test masses and have less crosstalk.

2. Mathematical Modeling of Mechanical Processes in OMIS

The analytical methods (see, for example, [12,13]) cannot be applied to describe mechanical processes in drum-type OMIS structures due to the relative complexity of their spatial configuration (see Figure 1a). So, it is necessary to use numerical methods, such as the finite element method. To model the OMIS mechanical characteristics, we use COMSOL Multiphysics 5.6. This package applies Newton's second law to calculate mechanical processes [14]. To consider the processes related to thermoelastic damping in linear viscoelastic materials, the generalized Kelvin–Voigt model was applied, which is recommended for describing processes in glassy polymers [15].

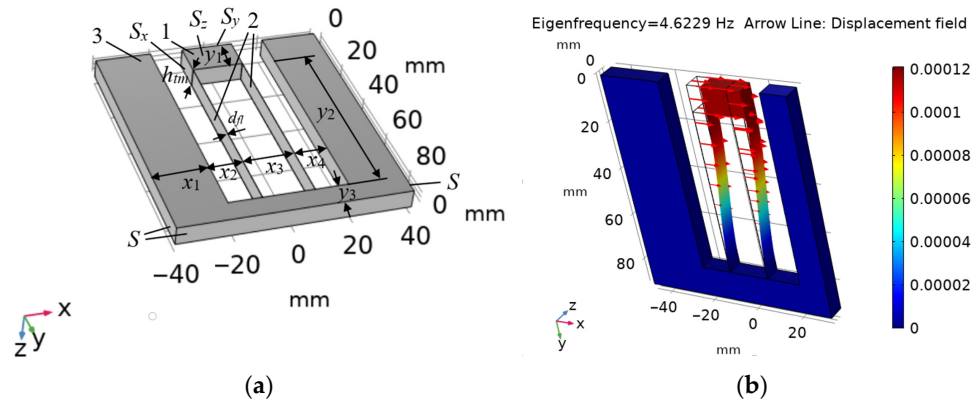


Figure 1. Modeling of the OMIS with in-plane design. (a) OMIS configuration [5]: $x_1 = 26$ mm, $x_2 = 12.5$ mm, $x_3 = 16.75$ mm, $x_4 = 14$ mm, $y_1 = 10.75$ mm, $y_2 = 67.5$ mm, $y_3 = 12.25$ mm, $h_{tm} = 6.6$ mm, $y_2 = 67.5$ mm, $h_{tm} = 6.6$ mm, $d_{fl} = 100$ μ m; (b) calculated displacement field mode for the first eigenfrequency $f_{ef1} = 4.6229$ Hz, red arrows show the displacement field.

The OMIS model of mechanical processes was tested by comparison with the experimental data presented elsewhere [5,9]. We investigated OMIS with the known in-plane design used for the measurement of accelerations with low frequencies [5] with a rectangular test mass 1 and flexes 2 connecting it with the constrained part 3 (see Figure 1a). A comparison of the experimental value of the natural frequency of OMIS with the values that we simulated in COMSOL Multiphysics 5.6 (see Figure 1b) showed that their relative difference does not exceed 2% (the experimental resonant frequency equals 4.715 Hz [5] versus the modeled level $f_{ef1} = 4.6229$ Hz).

Since no load is applied when calculating eigenfrequencies in the systems under consideration, the displacement levels indicated in the color captions of the calculated displacement mode shape refer only to the relative movement of different zones; consequently, the displacement units are not indicated on the color legend (see Figure 1b).

The model elaborated was used for the determination of the eigenfrequencies of the drum-type OMIS [9] (see Figure 2a). As a comparison of the simulated levels of the first three eigenfrequencies, namely $f_{ef1}, f_{ef2}, f_{ef3}$ (see Figure 2b–d) with the data from [9] shows, the relative differences in these levels are less than 2%, namely, $f_{ef1} = 1.0253$ kHz versus $f_{ef1} = 1.0139$ kHz [9], $f_{ef2} = 2.0627$ kHz versus $f_{ef2} = 2.0454$ kHz [9], and $f_{ef3} = 18.915$ kHz versus $f_{ef2} = 18.4$ kHz [9].

To analyze mechanical processes and compare the output characteristics of OMIS of different designs, we will use parameters called participation factors. We can write the displacement as a linear combination of the eigenmodes [14]:

$$u_k \approx \sum_{j=1}^n \hat{q}_{k,j} \cdot u_{k,j}, \quad (1)$$

where $\hat{q}_{k,j}$ is the amplitude of the (k,j) -th eigenmode; $u_{k,j}$ is the shape of the (k,j) -th eigenmode; j is the eigenmode number; n is the total number of eigenmodes; and k is the number of directions (corresponding to the x, y or z axes).

The amplitude of the (k,j) -th eigenmode is written as follows:

$$\hat{q}_{k,j} = \frac{S_{a,k} \cdot \Gamma_{k,j}}{\omega_j^2}, \quad (2)$$

where $S_{a,k} \approx \omega_0^2 \cdot S_{d,k}$ is the acceleration response spectra in the k -th direction (corresponds to the maximum acceleration value at the first eigenfrequency ω_0); $S_{d,k}$ is the displacement response spectra in the k -th direction (corresponds to the maximum displacement value at the first eigenfrequency); ω_j is the circular frequency of the j -th eigenmode; $\Gamma_{k,j}$ is the modal participation factor of the j -th eigenmode in the k -th direction.

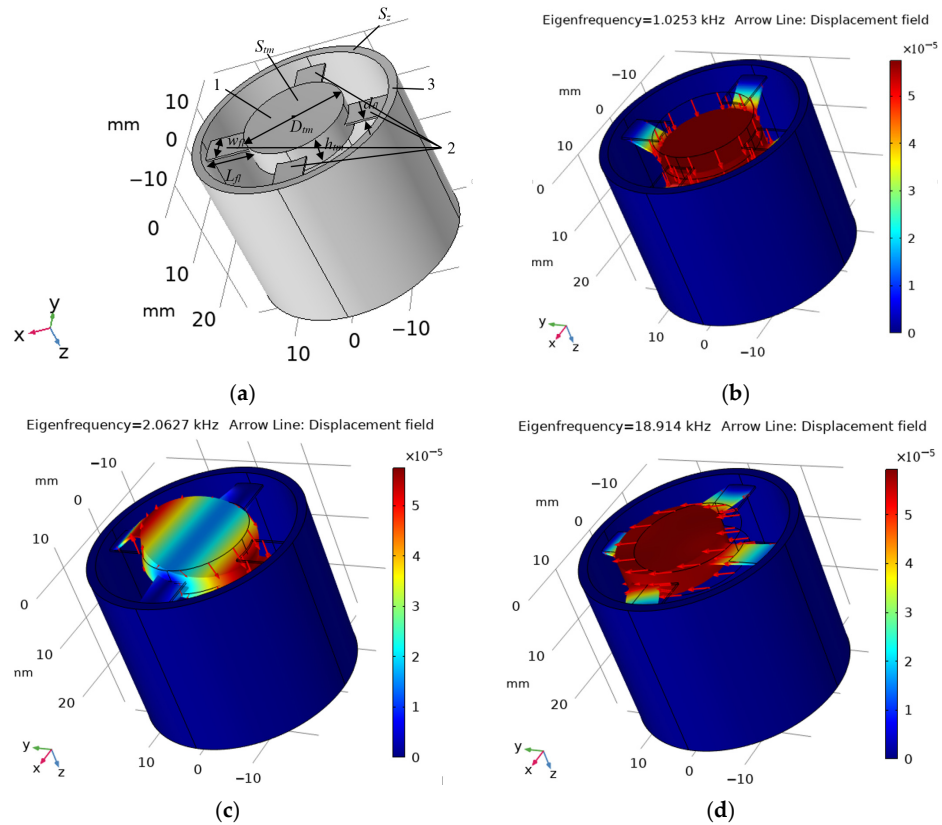


Figure 2. (a) Drum-type OMIS geometry [9]: 1—the OMIS test mass, on which a mirror for acceleration measurements is located, 2—four flexures, 3—the outer constrained cylinder, $D_{tm} = 17.3$ mm, $h_{tm} = 4.44$ mm, $L_{fl} = 7.6$ mm, $w_{fl} = 5$ mm, $d_{fl} = 310$ μ m; (b) $f_{ef1} = 1.0253$ kHz, (c) $f_{ef2} = 2.0627$ kHz, and (d) $f_{ef3} = 18.915$ kHz are calculated displacement mode shapes for the first three eigenfrequencies, red arrows show the displacement fields.

Let us rewrite (1) as follows:

$$u_k \approx \sum_{j=1}^n \Psi_{k,j} \cdot S_{d,k} \cdot u_{k,j}, \tag{3}$$

where

$$\Psi_{k,j} = (\omega_0^2 / \omega_j^2) \cdot \Gamma_{k,j} \tag{4}$$

The coefficient Ψ_{kj} characterizes the contribution of each displacement mode to the total displacement.

An important parameter characterizing OMIS performance is the level of crosstalk when movement in directions (for us, this is the x and y directions) perpendicular to the direction of acceleration measurement (for us, this is the z direction) also leads to the appearance of movements in the direction of its measurement. To assess this factor, we consider the degree of participation of movements in the x or y directions (these directions in the case under consideration are equivalent), introducing the coefficient Ψ^* . We assume that this coefficient is equal to the ratio of the coefficient $\Psi_{x,2}$ (see (4) at $k = x, j = 2$), which corresponds to the second natural frequency in the x direction, to the coefficient $\Psi_{z,1}$ (see (4) at $k = z, j = 1$), which corresponds to the first natural frequency ($\omega_0 = \omega_1$) in the z direction (in our case, this is the largest of all values $\Psi_{k,j}$):

$$\Psi^* = (\omega_0^2 / \omega_j^2) \cdot (\Gamma_{x,2} / \Gamma_{z,1}) \cdot 100\%.$$

This parameter is more informative than the commonly used coefficient of excess of the second natural frequency over the first: $K_{12} = f_{ef2} / f_{ef1}$ [3,5,8]. Unlike parameter K_{12} ,

Ψ^* gives a more complete picture of the degree of influence of movement in directions perpendicular to the direction in which acceleration is measured on the character of the resulting movement. For example, K_{12} can be rather large, but participation factors in the x and z directions can be almost equal. Or vice versa, f_{ef2} and f_{ef1} can be almost the same, and participation factors in the x direction can be orders of magnitude smaller than in the z direction. In these cases, the value of K_{12} does not give a correct idea of the degree of influence of crosstalk, but the parameter Ψ^* does.

3. OMIS Optical Readout Using the Fabry–Pérot Cavity

The optomechanical accelerometer allows the measured acceleration to be converted into a displacement of the test mass. Provided that the higher modes of the oscillator under study have frequencies significantly higher than its first natural frequency, this generator, for simplicity, can be represented as a single-mode harmonic oscillator. Then, the relationship between the measured acceleration $a(\omega)$, frequency ω , and the recorded displacement of the test mass $Z_{tm}(\omega)$ can be written as follows [1]:

$$a = Z_{tm}(\omega)/K(\omega), \tag{5}$$

$$K(\omega) = 1/(\omega_0^2 - \omega^2 + i\omega\omega_0/Q), \tag{6}$$

where Q is the mechanical quality factor; and ω_0 is the oscillator's natural frequency, coinciding with the first eigenfrequency; $i = \sqrt{-1}$.

If the frequency of the measured acceleration ω is significantly lower than the first eigenfrequency: $\omega \ll \omega_0$, then (6) can be written as follows:

$$K(\omega) \approx 1/\omega_0^2 \tag{7}$$

The level of displacement of the OMIS test mass is determined by an optical readout using the Fabry–Pérot cavity. The moving test mass is one of the mirrors of the Fabry–Pérot cavity, the second mirror of which is fixed relative to the test mass. To ensure the reflectivity of mirrors, they are polished and have coatings with reflectivity R_1 and R_2 . It is known that spectral analysis using the Fabry–Pérot cavity is based on the interference of the incident laser beam and beams reflected from the cavity mirrors. The time required for the beam to cross the cavity and return (t_{RT}) determines the value of the free spectral range:

$$\Delta\nu_{FSR} = 1/t_{RT} = c/2L,$$

where $c = 2.99792458 \cdot 10^8$ m/s.

The photon-decay time τ_c of the resonator can be presented as follows [16]:

$$\tau_c = -t_{RT}/\ln(R_1R_2).$$

Full width at half maximum (FWHM) linewidth of the Lorentzian spectral line shape:

$$\Delta\nu_c = (2\pi \cdot \tau_c)^{-1}.$$

The Lorentzian finesse of a Fabry–Pérot resonator is determined as follows [16]:

$$F_c = \Delta\nu_{FSR}/\Delta\nu_c = -2\pi/\ln(R_1R_2).$$

The movement of the test mass causes a change in the length of the Fabry–Pérot cavity, shifting the frequency of its optical resonance and modulating the amplitude of the electrical component of the electromagnetic field. The result of this is the appearance of a photocurrent that periodically changes with the frequency of mechanical vibrations ω [17]. The magnitude of the recorded voltage depends on the value of the movement of the test mass and is determined by the Airy function considering multiple reflections [3,18,19]. This

voltage also depends on the wavelength of the laser used, the reflectivity of the Fabry–Pérot cavity mirrors, and losses in the system.

Neglecting losses, we write down the relationship between the ratio of the movement of the test mass Z_{tm} to the length of the Fabry–Pérot cavity L and the ratio of the laser tuning range $\Delta\nu_L$ to its frequency $\nu_L = c/\lambda_L$:

$$Z_{tm}/L = \Delta\nu_L/\nu_L.$$

From here, we determine the value of the maximum measured movement of the test mass, $Z_{tm \max}$ [20]:

$$Z_{tm\max} = (L/\nu_L) \cdot \Delta\nu_L. \tag{8}$$

For the system under consideration, the reflectivity of the Fabry–Pérot cavity mirrors R_1 and R_2 should be equal to or better than 0.9997 to obtain a rather large finesse. The planned distance between the mirrors is $L = 22$ mm, a laser with a wavelength of $\lambda_L = 780$ nm and a tuning range of a few GHz (1 GHz is approximately equal to $g = 9.81$ m/s of acceleration) is used. Then, $\Delta\nu_{FSR} = 6.8$ GHz, $\tau_c = 0.245$ μ s, $\Delta\nu_c = 0.65$ MHz, $F_c \approx 10^4$ and, therefore, $Z_{tm \max} \approx 60$ nm.

From the above data, it follows that increasing the first natural frequency of a mechanical resonator ω_0 above the level necessary for measuring the acceleration of an assigned frequency ω , namely $\omega_0 \approx 10 \cdot \omega$, is inappropriate since this leads to an unnecessary decrease in the level of displacement of the test mass when measuring accelerations (see (5), (7), (8)) and requires increasing the accuracy of measuring this displacement.

4. Choosing a Miniature OMIS Design to Ensure Functional Properties and Its Manufacturing

When choosing an OMIS design, it should be considered that its samples are made, as a rule, using laser cutting and etching. The frontal surface S_{tm} of the OMIS test mass 1 (see Figure 2a), which serves as one of the mirrors of the Fabry–Pérot cavity when optically reading its movement, must be polished to a high degree of homogeneity after the OMIS is cut out in order to achieve the necessary finesse.

To ensure such high-quality polishing, δ_r , the distance between the test mass 1 and the external fixed hollow cylinder 3 in the radial direction should be small. But for the drum-type OMIS design depicted elsewhere [9] (see Figure 2a), this distance is equal to the length w_{fl} of the flexures 2 connecting the test mass 1 with the external fixed part 3. A decrease in w_{fl} leads to a significant increase in f_{ef1} —the first eigenfrequency of OMIS. The necessary value of f_{ef1} is determined by the level of the upper limit of the required range of measured accelerations $f_{op \max}$:

$$f_{ef1} \approx 10 \cdot f_{op \max}$$

and as shown above, increasing f_{ef1} above this value is not advisable.

To reduce the distance between the OMIS test mass 1 and the external fixed structure 3, the following design was developed (see Figure 3a). This design involves increasing the length of flexures 2 by making them in the form of arc segments parallel to the side surfaces of the cylindrical test mass 1. Due to this, the rigidity of the structure is reduced, and the first natural frequency becomes smaller. The number of flexures in the proposed design has been reduced from four (see Figure 2a) to three (see Figure 3a). Let us set the dimensions of OMIS with the design described in [9], the same as for OMIS of the proposed design (see Figure 3a), namely $D_{tm} = 6$ mm, $h_{tm} = 2.7$ mm, $L_{fl} = \delta_r = 1.5$ mm, $w_{fl} = 1$ mm, and $d_{fl} = 200$ μ m. As can be seen from the comparison of the simulated displacement mode shapes for the first eigenfrequency for the OMIS of the design described elsewhere [9] (see Figure 2c) with the OMIS of the proposed design (see Figure 3b), the latter allows for a reduction in the first eigenfrequency from 9.626 kHz to 2.0874 kHz.

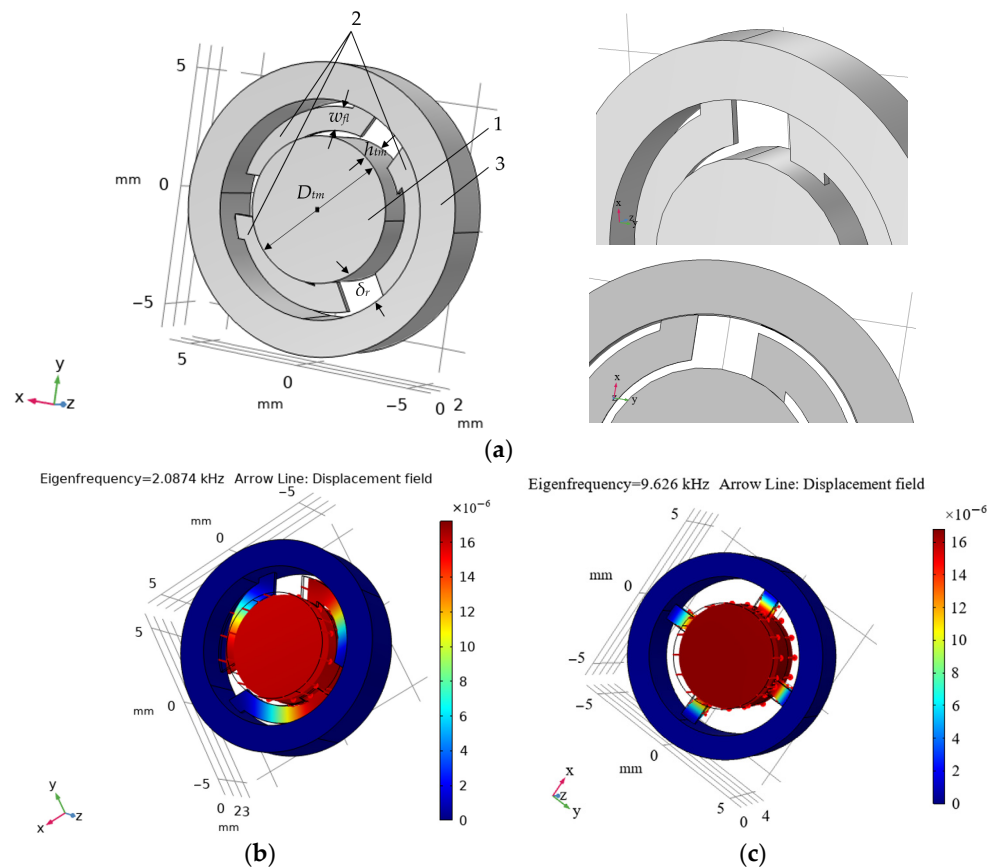


Figure 3. (a) Design of OMIS with three curved flexures and enlarged parts of the flexures that connect the movable part of the OMIS to its fixed part; calculated displacement mode shape for the first eigenfrequency; (b) OMIS with three curved flexures $f_{ef1} = 2.0874$ kHz; (c) OMIS design [9] with four straight flexures $f_{ef1} = 9.626$ kHz. Red arrows show the displacement fields.

However, the OMIS of the described design has some crosstalk since the maximum value of coefficient Ψ^* is relatively large: $\Psi^* = 2.7\%$. To reduce this crosstalk, the design is modified so that instead of three flexures, an OMIS has six flexures (see Figure 4a). We propose to make the length of these flexures, L_{flr} , approximately equal to L_{gpr} , the length of the distance between them. An OMIS of this design can be made as follows: first, from a piece of fused quartz, using laser cutting, we obtain a cylinder, with the contour of the outer contour of constrained cylinder 3. Then, also using laser cutting, the contour of the test mass 1 and the contours of the flexures 2 can be cut out so that all elements of the structure have a thickness of h_{tm} . After this, the spaces 4 can be etched so that the flexures 2 have a thickness of $d_{fl} < h_{tm}$ (see Figure 4a). The modeled displacement mode shape for the first eigenfrequency for such an OMIS is shown in Figure 4b. Such a design provides a smaller maximum value of coefficient Ψ^* , namely $\Psi^* = 1\%$.

To reduce further crosstalk and enable high-quality polishing of the test mass front surface, we propose one more OMIS design shown in Figure 5. When manufacturing such an OMIS, a cylinder Cyl with a diameter of D_{out} and a height of h_{tm} is cut out from a single piece of fused silica, for example, using a laser. Considering that only the front surface of the test mass S_{fr} (see Figure 5a) must be polished and the rear surface of the test mass S_b (see Figure 5b) is not, the rear base of the cylinder Cyl should not have a solid surface. The manufacturing of OMIS from a cylinder is started by etching or laser cutting out the test mass 1 and the contours of three flexures 2 to a depth equal to $h_{tm} - d_{fl}$ (where h_{tm} is the height of the test mass in the z-axis direction, d_{fl} is the thickness of the flexures) so that the cylinder Cyl remains not cut through and has a bottom of thickness d_{fl} in front of the front base (see Figure 5b). Some material in the area between the top and bottom

bases of the cylinder is then etched away, leaving a solid test mass 1 shaped like a cylinder of diameter D_{tm} and thickness h_{tm} , and three thin flexures 2 of thickness d_{fl} at the rear base (see Figure 5b). Then, in the upper base, slots are cut using a laser, outlining the contours of the test mass 1 and flexures 4, connecting them with the external constrained contour 3 (see Figure 5a). The width of the slots is δ_{sl} . Flexures 4 connecting the front base of the test mass 1 with the constrained OMIS outer part 3 (see Figure 5a) and flexures 2 connecting the front base of the test mass 1 with the constrained OMIS outer part 3 (see Figure 5b) are identical. They have length L_{fl} , width w_{fl} , and thickness d_{fl} . To reduce the swaying of the Section 5 of the frontal base of test mass (see Figure 5a) at the second and subsequent eigenfrequencies, it is proposed to leave small uncut sections—belts with width δ_{band} —between zones 5 and flexures 4 (see 6 in Figure 5d).

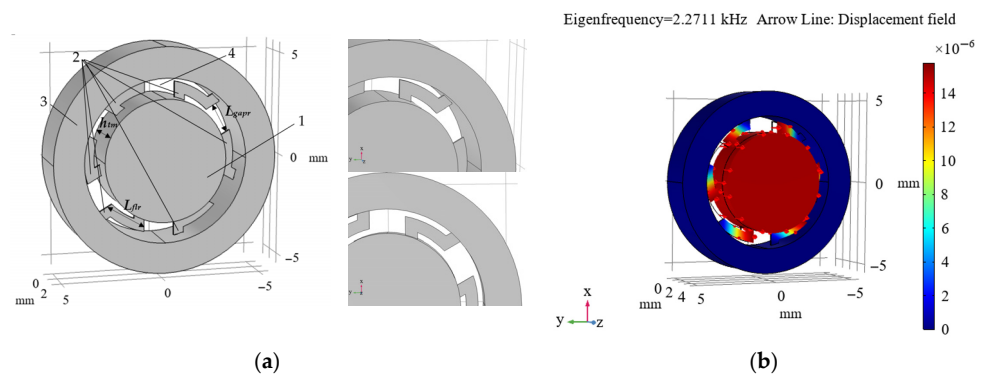


Figure 4. (a) Design of OMIS with six curved flexures and enlarged parts of the flexures that connect the movable part of the OMIS to its fixed part; (b) calculated displacement mode shape for the first eigenfrequency $f_{ef1} = 2.2543$ kHz. Red arrows show the displacement field.

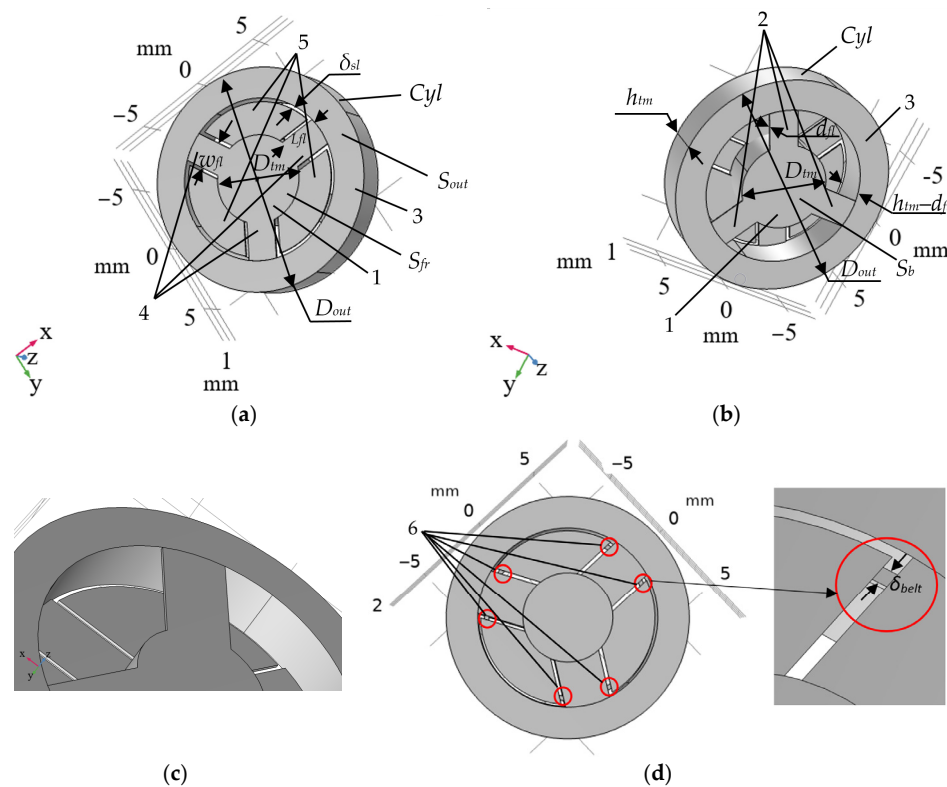


Figure 5. Proposed OMIS design: (a) front view, (b) rear view, (c) enlarged parts of the flexures that connect the movable part of the OMIS to its fixed part (rear view); (d) OMIS design with belts (parts 6 in red circles).

5. Analysis of the Mechanical Characteristics of the OMIS of the Proposed Design

The proposed optomechanical acceleration sensor design (see Figure 5) can be used to measure accelerations at different frequencies. Let us consider how the geometric parameters of the OMIS of a given design influence its output characteristics. To do this, we use mathematical modeling of mechanical processes in the systems under consideration. It is advisable to carry out such modeling before the start of manufacturing because the production of miniature OMIS is a complex and expensive process. Moreover, a number of parameters, such as the levels of higher natural frequencies and the magnitude of crosstalk, are difficult to obtain experimentally. In addition, some characteristics, namely the shape of displacement modes, participation factors, and the character of displacements in different directions, can only be simulated as a rule.

During modeling, we will assume that the diameter of the test mass is given and equal to $D_{tm} = 6$ mm. This miniature size is due to the intended use of OMIS for space missions. As shown by previous studies [11,21,22], as well as by preliminary calculations, the parameters that most influence the output characteristics of OMIS are the thickness and length of flexures 2, 4, the thickness of the test mass 1, as well as δ_{sl} , the size of the gap between test mass 1 and the constrained outer part of OMIS 3 (see Figure 5). As a basic variant, we will use an OMIS with the following parameters: the test mass with a diameter $D_{tm} = 6$ mm, thickness $h_{tm} = 2.7$ mm, mass $m = S_{tm} \cdot \pi \cdot (D_{tm}/2)^2 \cdot h_{tm} = 0.168$ mg ($\rho_{fs} = 2203$ kg/m³ is density of fused silica), flexures length $L_{fl} = 3.5$ mm, width $w_{fl} = 3$ mm, and flexures thickness $d_{fl} = 100$ μ m. Other parameters are as follows: $\delta_{sl} = \delta_{band} = 250$ μ m, $D_{out} = 17$ mm.

Figure 6 shows the calculated distributions of the first and second displacement modes for OMIS with the parameters described above. As can be seen from the distribution (see Figure 6a), for the first mode, the main type of motion is movement in the direction of the z axis, along which the acceleration is measured. The second mode, whose eigenfrequency is four times higher than the first eigenfrequency, corresponds to the vibration of technological parts 5 (see Figure 5a). However, this mode does not affect the main type of motion because its participation factor value is more than three orders of magnitude less than for the first eigenfrequency (see Figure 7). Thus, the total contribution of the motion corresponding to the second eigenfrequency does not exceed one-hundredths of a percent of the level of contribution of the mode of motion corresponding to the first eigenfrequency.

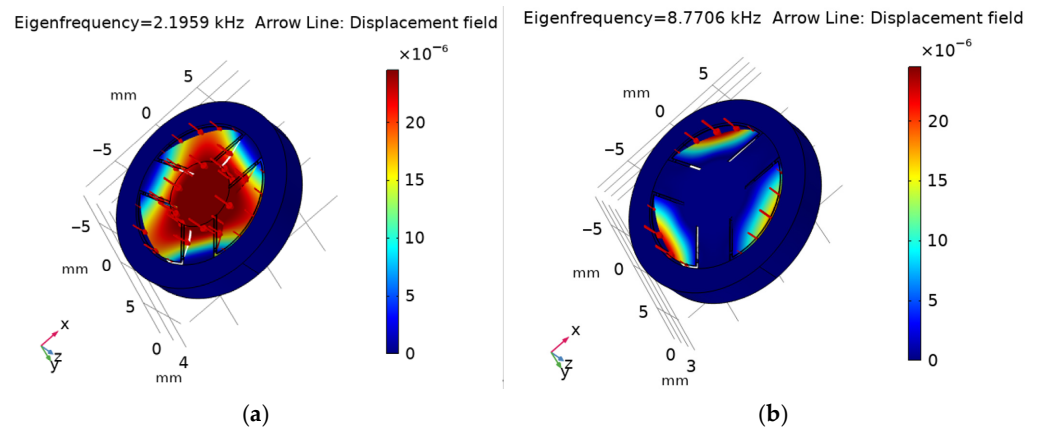


Figure 6. Calculated displacement modes for the first (a) $f_{ef1} = 2.1959$ kHz and second (b) $f_{ef2} = 8.7706$ kHz eigenfrequencies for the OMIS design from Figure 5d. Red arrows show the displacement fields.

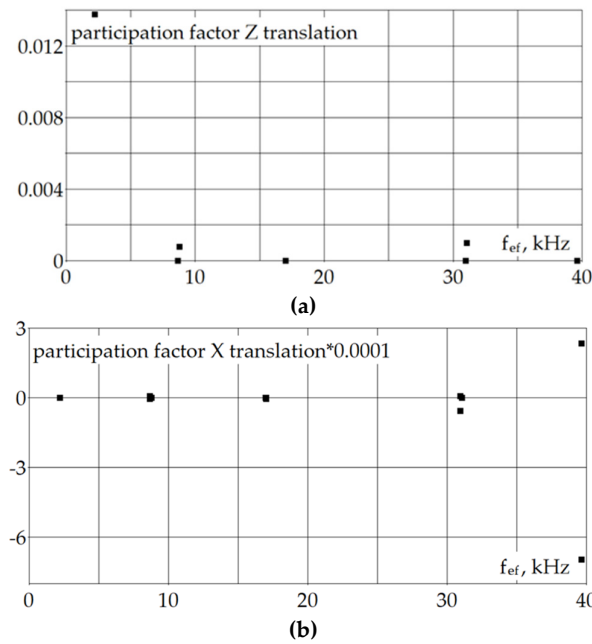


Figure 7. Calculated normalized participation factors of the Z (a) and X (b) translations versus eigenfrequencies (each square corresponds to a participation factor level at a certain eigenfrequency) for the OMIS design from Figure 5d.

As shown by the simulation, when δ_{sl} changes within the range of 250–1000 nm, the first natural frequency changes by no more than 1.4%. The second natural frequency increases with increasing δ_{sl} , but the coefficient Ψ^* , characterizing the contribution of this frequency to the total displacement, remains less than 0.1%.

Figure 8 shows the calculated dependences of f_{ef1} on the length of flexures L_{fl} (Figure 8a), their thickness d_{fl} (Figure 8b), their width w_{fl} (Figure 8c), as well as the test mass thickness h_{tm} (Figure 8d). As can be seen from these dependencies, the greatest influence on the f_{ef1} value is caused by the length and thickness of the flexures. As can be seen from Figure 8d, varying h_{tm} does not lead to a significant change in f_{ef1} . As follows from the calculations performed, the coefficient Ψ^* remains very small at all levels of varying geometric parameters of OMIS and does not exceed 0.1%. This means that the influence of higher harmonics is negligible for the OMIS of the proposed design, which means there is practically no crosstalk.

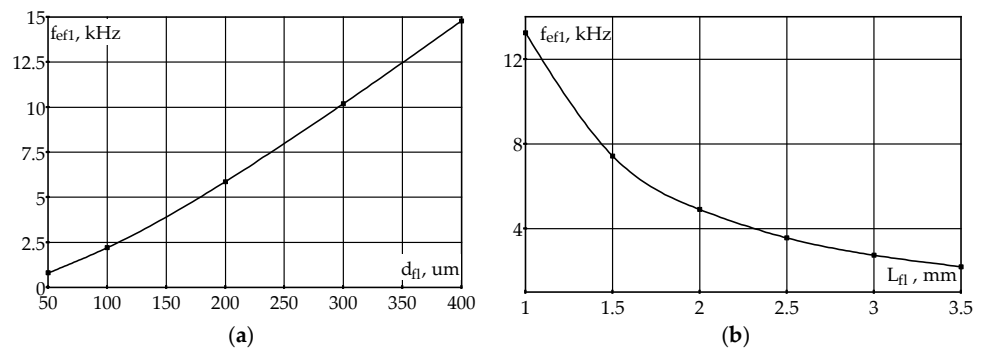


Figure 8. Cont.

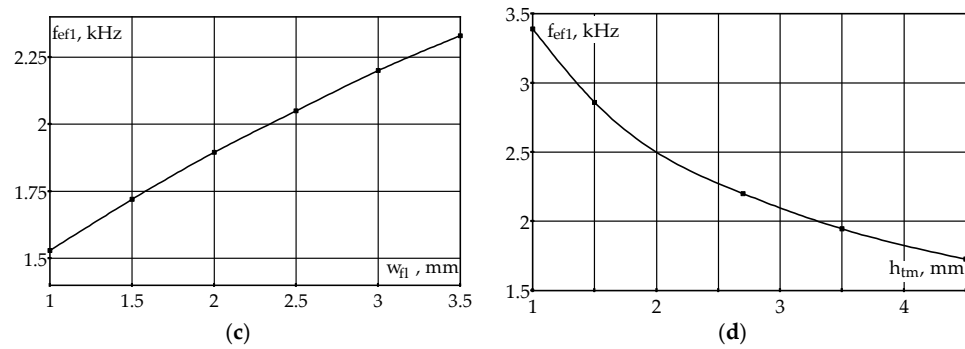


Figure 8. Calculated distributions of the first eigenfrequency (f_{ef1}) versus OMIS parameters: (a) $f_{ef1}(d_{fl})$; (b) $f_{ef1}(L_{fl})$; (c) $f_{ef1}(w_{fl})$; (d) $f_{ef1}(h_{tm})$ for the OMIS design from Figure 5d.

6. Conclusions

To ensure the measurement of accelerations with frequencies of hundreds of hertz, a drum-type OMIS with an improved design was proposed. For this purpose, a new OMIS design was developed, which involves connecting a cylindrical movable test mass with the OMIS constrained part using six thin flexures, three of which connect the front base of the test mass and three to its rear base. The front base of the test mass, which serves as a movable mirror of the Fabry–Perot cavity when measuring acceleration, has a common surface with the front base of the constrained cylinder. A narrow contour is cut out of this surface, outlining three flexures and circle segments separating the moving test mass from the constrained cylinder. Three more flexures connecting the rear base of the test mass to the rear base of the constrained cylinder are shifted on an angle of 60° relative to the front flexures (see Figure 5). This design is technologically advanced because it makes it relatively easy to manufacture such an OMIS and control its dimensions, as well as provide better polishing of the front base of the OMIS. This design ensures high-quality polishing due to the almost continuous front surface of the OMIS, which includes its moving and fixed parts. This design provides the required first eigenfrequency of about 2 kHz and reduces crosstalk.

Another OMIS for drum design was also developed. It is proposed to attach the test mass to the external constrained contour using arc-shaped thin flexures extended along the outer cylindrical contour of the test mass (see Figure 4). An OMIS of this design also provides the necessary first eigenfrequency of the order of 2 kHz, has a relatively simple design, allows for polishing of the frontal base of the test mass, which serves as a mirror in the Fabry–Perot resonator, and can be manufactured using laser cutting and etching. This polishing is possible because the size of the gap between the test mass and the external fixed part of the OMIS is significantly reduced compared to existing drum type structures (see Figures 3 and 4).

The choice of OMIS design is primarily determined by the frequency range of the measured acceleration. If the measured acceleration changes slowly (frequencies of the order of a few hertz), then it is preferable to use the so-called in-plane OMIS [1,5,8] (see Figure 1). This configuration consists of a movable test mass attached to a fixed outer frame using thin flexures. This design is simple and technologically advanced since it allows for manufacturing from a single block of fused silica, for example, using laser cutting. However, OMIS of this design has a limitation on the upper frequency [22]. Therefore, if it is necessary to measure rapidly changing accelerations (frequencies of the order of hundreds of hertz or more), the so-called out-of-plane OMIS or drum-type OMIS is usually used [5,9,21,22] (see Figures 2a, 3a, 4a and 5a). When choosing a drum-type OMIS design, one more factor should be considered, namely the possibility of polishing the front surface of the OMIS test mass (see S_{fr} in Figure 5a), which serves as one of the mirrors of the Fabry–Perot cavity when optically reading the movement of the test mass. To ensure such polishing, the distance between the test mass (see 1 in Figures 2a, 3a and 4a) and the outer constrained cylinder (see 3 in Figures 2a, 3a and 4a) must be as small as possible. This

is possible if the length of the flexures (see 2 in Figures 2a, 3a and 4a) is short. However, reducing the length of flexures when using the existing OMIS design [9] leads to an increase in natural frequency (see Figure 3c), which is impractical. To increase the length of flexures without increasing the natural frequency, it is proposed to make the flexures curved along the lateral surface of the test mass (see Figures 3a and 4a). An OMIS of this design is more complex to manufacture than the OMIS described in [9], but due to its relatively simple configuration, visual inspection and control of the dimensions of its parts is possible. The disadvantage of this OMIS design is the limited natural frequency values due to the impossibility of varying the length of the flexures over a wide range. Another OMIS design that provides the ability to polish the frontal base of the test mass is a design with a cut technological surface between this base and the outer constrained cylinder (see Figure 5). The advantage of this design OMIS is the absence of crosstalk, as well as the ability to vary the natural frequency over a wide range by varying the length of the flexures. OMIS of this design is even more complex to manufacture but also provides visual inspection and control of the dimensions of its parts.

Author Contributions: M.R. performed mathematical modeling, data curation, writing, review, and editing. C.B. conceptualized and supervised the study. All authors have read and agreed to the published version of the manuscript.

Funding: This work is supported by the German Space Agency (DLR e.V.), with funds provided by the Federal Ministry of Economic Affairs and Climate Action, under grant number 50WM2262B (HyQIS), BMBF by future cluster QSENS (project 03ZU1110JA QSPACE).

Data Availability Statement: The data presented in this study are available upon request from the corresponding author.

Conflicts of Interest: The authors declare no conflicts of interest.

References

1. Reschovsky, B.J.; Long, D.A.; Zhou, F.; Bao, Y.; Allen, R.A.; LeBrun, T.W.; Gorman, J.J. Intrinsically accurate sensing with an optomechanical accelerometer. *Opt. Express* **2022**, *30*, 19510–19523. [CrossRef]
2. Abozyd, S.; Toraya, A.; Gaber, N. Design and Modeling of Fiber-Free Optical MEMS Accelerometer Enabling 3D Measurements. *Micromachines* **2022**, *13*, 343. [CrossRef]
3. Guzmán Cervantes, F.; Kumanchik, L.; Pratt, J.; Taylor, J.M. High sensitivity optomechanical reference accelerometer over 10 kHz. *Appl. Phys. Lett.* **2014**, *104*, 221111. [CrossRef]
4. Noureldin, A.; Karamat, T.B.; Georgy, J. *Fundamentals of Inertial Navigation, Satellite-Based Positioning and Their Integration*, 1st ed.; Springer: Berlin, Germany, 2013.
5. Hines, A.; Nelson, A.; Zhang, Y.; Valdes, G.; Sanjuan, J.; Stoddart, J.; Guzmán, F. Optomechanical Accelerometers for Geodesy. *Remote Sens.* **2022**, *14*, 4389. [CrossRef]
6. Hines, A.; Richardson, L.; Wisniewski, H.; Guzman, F. Optomechanical inertial sensors. *Appl. Opt.* **2020**, *59*, G167–G174. Available online: <https://opg.optica.org/ao/abstract.cfm?URI=ao-59-22-G167> (accessed on 14 May 2024). [CrossRef] [PubMed]
7. Melcher, J.; Stirling, J.; Cervantes, F.G.; Pratt, J.R.; Shaw, G.A. A self-calibrating optomechanical force sensor with femtonewton resolution. *Appl. Phys. Lett.* **2014**, *105*, 233109. [CrossRef]
8. Guzmán, F.; Kumanchik, L.; Spannagel, R.; Braxmaier, C. Compact fully monolithic optomechanical accelerometer. *arXiv* **2018**, arXiv:1811.01049.
9. Richardson, L.; Hines, A.; Schaffer, A.; Anderson, B.P.; Guzmán, F. Quantum hybrid optomechanical inertial sensing. *Appl. Opt.* **2020**, *59*, G160–G166. [CrossRef] [PubMed]
10. Carter, J.J.; Birckigt, P.; Gerberding, O.; Koehlenbeck, S.M. High Precision Inertial Sensors on a One Inch Diameter Optic. *arXiv* **2024**, arXiv:2403.12632. [CrossRef]
11. Kumanchik, L.; Rezinkina, M.; Braxmaier, C. Choice of the miniature inertial optomechanical sensor geometric parameters with the help of their mechanical characteristics modelling. *Micromachines* **2023**, *14*, 1865. [CrossRef] [PubMed]
12. Low, K.H. A comparative study of the eigenvalue solutions for mass-loaded beams under classical boundary conditions. *Int. J. Mech. Sci.* **2001**, *43*, 237–244. [CrossRef]
13. Gürgöze, M. On the eigenfrequencies of cantilevered beams carrying a tip mass and spring-mass in-span. *Int. J. Mech. Sci.* **1996**, *38*, 1295–1306. [CrossRef]
14. Structural Mechanics Module. User's Guide 1998–2018. COMSOL. Available online: <https://doc.comsol.com/5.4/doc/com.comsol.help.sme/StructuralMechanicsModuleUsersGuide.pdf> (accessed on 16 February 2023).

15. Linear Viscoelastic Materials. Available online: https://doc.comsol.com/5.6/doc/com.comsol.help.sme/sme_ug_theory.06.26.html (accessed on 16 February 2023).
16. Ismail, N.; Kores, C.C.; Geskus, D.; Pollnau, M. Fabry-Pérot resonator: Spectral line shapes, generic and related Airy distributions, linewidths, finesses, and performance at low or frequency-dependent reflectivity. *Opt. Express* **2016**, *24*, 16366–16389. [[CrossRef](#)] [[PubMed](#)]
17. Li, B.-B.; Ou, L.; Lei, Y.; Liu, Y.-C. Cavity optomechanical sensing. *Nanophotonics* **2021**, *10*, 2799–2832. [[CrossRef](#)]
18. Santos, J.L.; Leite, A.P.; Jackson, D.A. Optical fiber sensing with a low-finesse Fabry-Perot cavity. *Appl. Opt.* **1992**, *31*, 7361–7366. [[CrossRef](#)] [[PubMed](#)]
19. Gerberding, O.; Guzmán Cervantes, F.; Melcher, J.; Pratt, J.R.; Taylor, J.M. Optomechanical reference accelerometer. *Metrologia* **2015**, *52*, 654–665. [[CrossRef](#)]
20. Zhang, Y.; Hines, A.; Wilson, D.J.; Guzman, F. Optomechanical cooling and inertial sensing at low frequencies. *Phys. Rev. Appl.* **2023**, *19*, 054004. [[CrossRef](#)]
21. Carter, J.; Köhlenbeck, S.; Birckigt, P.; Eberhardt, R.; Heinzl, G.; Gerberding, O. A High Q, Quasi-Monolithic Optomechanical Inertial Sensor. In Proceedings of the 2020 IEEE International Symposium on Inertial Sensors and Systems (INERTIAL), Hiroshima, Japan, 23–26 March 2020; pp. 1–4. [[CrossRef](#)]
22. Rezinkina, M.; Braxmaier, C. Designs of Optomechanical Acceleration Sensors with the Natural Frequency from 5 Hz to 50 kHz. *Designs* **2024**, *8*, 33. [[CrossRef](#)]

Disclaimer/Publisher’s Note: The statements, opinions and data contained in all publications are solely those of the individual author(s) and contributor(s) and not of MDPI and/or the editor(s). MDPI and/or the editor(s) disclaim responsibility for any injury to people or property resulting from any ideas, methods, instructions or products referred to in the content.